

## MATERIALS SCIENCE

# A nonconjugated radical polymer enables bimodal memory and in-sensor computing operation

Jaehyoung Ko<sup>1,2</sup>, Daeun Kim<sup>1,3</sup>, Quynh H. Nguyen<sup>1</sup>, Changhyeon Lee<sup>2</sup>, Namju Kim<sup>4</sup>, Hoyeon Lee<sup>1,2</sup>, Joohwan Eo<sup>1,5</sup>, Ji Eon Kwon<sup>1,6</sup>, Seung-Yeol Jeon<sup>1</sup>, Byung Chul Jang<sup>4\*</sup>, Sung Gap Im<sup>2\*</sup>, Yongho Joo<sup>1,7\*</sup>

This study reports intrinsic multimodal memristivity of a nonconjugated radical polymer with ambient stability. Organic memristive devices represent powerful candidates for biorealistic data storage and processing. However, there exists a substantial knowledge gap in realizing the synthetic biorealistic systems capable of effectively emulating the cooperative and multimodal activation processes in biological systems. In addition, conventional organic memristive materials are centered on conjugated small and macromolecules, making them synthetically challenging or difficult to process. In this work, we first describe the intrinsic resistive switching of the radical polymer that resulted in an exceptional state retention of  $>10^5$  s and on/off ratio of  $>10^6$ . Next, we demonstrate its bimodal cooperative switching, in response to the proton accumulation as a biological input. Last, we expand our system toward an advanced in-sensor computing system. Our research demonstrates a nonconjugated radical polymer with intrinsic memristivity, which is directly applicable to future electronics including data storage, neuromorphics, and in-sensor computing.

Copyright © 2024 The Authors, some rights reserved; exclusive licensee American Association for the Advancement of Science. No claim to original U.S. Government Works. Distributed under a Creative Commons Attribution NonCommercial License 4.0 (CC BY-NC).

## INTRODUCTION

Memristive devices have garnered considerable attention as promising candidates for future memory and computing applications (1, 2). These devices are capable of emulating synaptic functions, facilitating the development of neuromorphic systems (3, 4). Among these, organic memristive devices stand out due to their low-power operation, tunable multifunctionality, and affordability (5–8). Notably, the flexibility and biocompatibility inherent in organic materials are expected to enable the creation of real-life neuromorphic architectures, such as body-computer integration (5, 9). Nevertheless, a substantial knowledge gap exists within the current biorealistic systems. Biological systems often exploit cooperative and multimodal activation processes in their signal transduction (10, 11). This feature, exemplified by concerted activation in neuronal synapses through the cooperation between neurotransmitters and ions (e.g., protons) (12), has been rarely understood or successfully reproduced. The solution to this challenge lies in the development of a biorealistic device system capable of multimodal memristive operation (possibly from both ionic and electronic inputs), in which organic memristive devices find their unique advantages.

Conventionally, organic memristive devices have relied predominantly on conjugated polymers (6, 8). Despite their excellent conductivity and widely tunable electronic properties (13–15), they have

some inherent limitations (16, 17). First, conjugated polymers typically have poor solubility toward common organic solvents. This is detrimental to their general processing into devices and to the established scalable manufacturing techniques (e.g., inkjet printing). Second, the synthesis of advanced conjugated polymers can be challenging, often with low yields. This is substantiated by recent trends in many applications, such as biorealistic data processing, which are increasingly demanding polymers with highly multifunctional nature. Third, chemical doping strategy often adopted for the improved device performance of the conjugated polymer based memory can lead to device-to-device variability and may negatively affect the overall device stability (18).

Organic nonconjugated conductors, such as radical polymers, can offer an optimal solution to these challenges. In general, radical polymers consist of hydrocarbon backbone and pendant radicals with ambient stability (18, 19). Charge transport in radical polymers occurs through consecutive hopping of charge carriers between highly localized radical sites, in both an intramolecular and intermolecular fashion (16). In addition, a recent breakthrough in solid-state electrical conductivity of a radical polymer comparable to that of the doped conjugated polymers (17) underscores its potential as an exceptional organic conductor. Radical polymers can be inherently memristive due to the variable redox states of constituent radicals (20). While these features have recently been highlighted in a class of small-molecule radicals, macromolecular radicals with inherent memristivity have rarely been reported. Furthermore, radical polymers are suitable in reproducing the aforementioned biorealistic multimodality by facile molecular engineering of the hydrocarbon backbone into the ionic functionality (18). These features of radical polymers endow them with exceptional memory performance and multimodality comparable to the existing conjugated polymers, without compromising their superior processability, synthetic simplicity, and a single-component nature (i.e., no need for doping) (16, 21).

In this work, we demonstrate a multimodal memristivity of a radical polymer-based device: a bimodal resistive switching and an

<sup>1</sup>Institute of Advanced Composite Materials, Korea Institute of Science and Technology (KIST), Wanju-gun, Jeonbuk 55324, Republic of Korea. <sup>2</sup>Department of Chemical and Biomolecular Engineering, Korea Advanced Institute of Science and Technology (KAIST), Daejeon 34141, Republic of Korea. <sup>3</sup>School of Materials Science and Engineering, Gwangju Institute of Science and Technology, Gwangju 61005, Republic of Korea. <sup>4</sup>School of Electronic and Electrical Engineering, Kyungpook National University, Daegu 41566, Republic of Korea. <sup>5</sup>Department of Materials Science and Engineering, Seoul National University, 1 Gwanak-ro, Gwanak-gu, Seoul 08826, Republic of Korea. <sup>6</sup>Department of JBNU-KIST Industry Academia Convergence Research, Jeonbuk National University, 567 Baekje-daero, Deokjin-gu, Jeonju, Jeonbuk 54896, Republic of Korea. <sup>7</sup>Division of Nano and Information Technology, KIST School, Korea University of Science and Technology (UST), Jeonbuk 55324, Republic of Korea.

\*Corresponding author. Email: bc.jang@knu.ac.kr (B.C.J.); sgim@kaist.ac.kr (S.G.I.); yjoo0727@kist.re.kr (Y.J.)

in-sensor computing system therefrom. Specifically, we demonstrate that the variable redox states of a model radical polymer offer bistability for reliable resistive switching; we further illustrate that a neurotransmitter analog, such as proton, can also effectively modulate the switching behavior and even lead to a cooperative resistive switching; last, we describe the memristivity of the radical polymer upon its proton accumulation, which is, in turn, applied to an in-sensor computing module. Our demonstration here illustrates radical polymers with intrinsic multimodal memristivity, which greatly expands the base of such materials in next-generation data processing technology.

## RESULTS

Figure 1 presents an overview of our model radical polymer-based multimodal device operation. Briefly, the radical polymer in this study is capable of transporting charges through redox hopping (16). In addition, we used polar moieties on the backbone to facilitate ion transport of the system on demand (not shown for clarity). The radical polymer-based metal-insulator-metal (MIM) device displays multimodal memristivity, stimulated by electric fields in cooperation with proton accumulation. The device can be adapted to a humidity-dependent in-sensor computing system that directly processes external inputs, as opposed to the conventional sensory system characterized by the physical separation of sensor, memory, and processor units.

Securing a high concentration of active sites is of critical importance in the synthetic design of radical polymers with superior

electrical conductivity. Specifically, the electrical conductivity of a radical polymer is shown to exponentially increase with respect to the site density (22, 23). A widely recognized approach for preserving the active radical sites is direct polymerization of radical monomers, compared to the deprotection methods (24–27). The radical polymer used in this study, which is expected to exhibit electrical bistability for resistive switching and ionic sensitivity for multimodality, is one of the representatives of radical polymers, poly(4-glycidyloxy-2,2,6,6-tetramethylpiperidine-1-oxyl) (PTEO). Its synthesis follows an anionic ring-opening polymerization of a monomeric 2,2,6,6-tetramethylpiperidine-1-oxyl (TEMPO) derivative (28). The synthesis occurs under ambient conditions, resulting in PTEO having number-average molecular weight ( $M_n$ ) of ~14 kg mol<sup>-1</sup>, with the dispersity ( $D$ ) of 1.87 at a very high yield of >95% [synthetic characterization including nuclear magnetic resonance (NMR) and gel permeation chromatography and basic absorption characteristics of PTEO are detailed in the Supplementary Materials as figs. S1 to S4]. The polymer is capable of transporting both electrical and ionic charges through the pendant groups and the polar moieties of ethylene oxide, respectively (i.e., mixed conduction) (Fig. 2) (18). Specifically, the former is enabled via a series of self-exchange redox reactions between pendant radicals of close proximity (Fig. 2A) (17), while the latter is achieved by the ion solubility endowed by the lone pair electrons of the oxygen in the backbone (Fig. 2B) (18). To provide more insights into the charge transport behavior in PTEO, we conducted a molecular dynamics (MD) simulation consisting of 100 pentamers (Fig. 2, C to E). The optimized

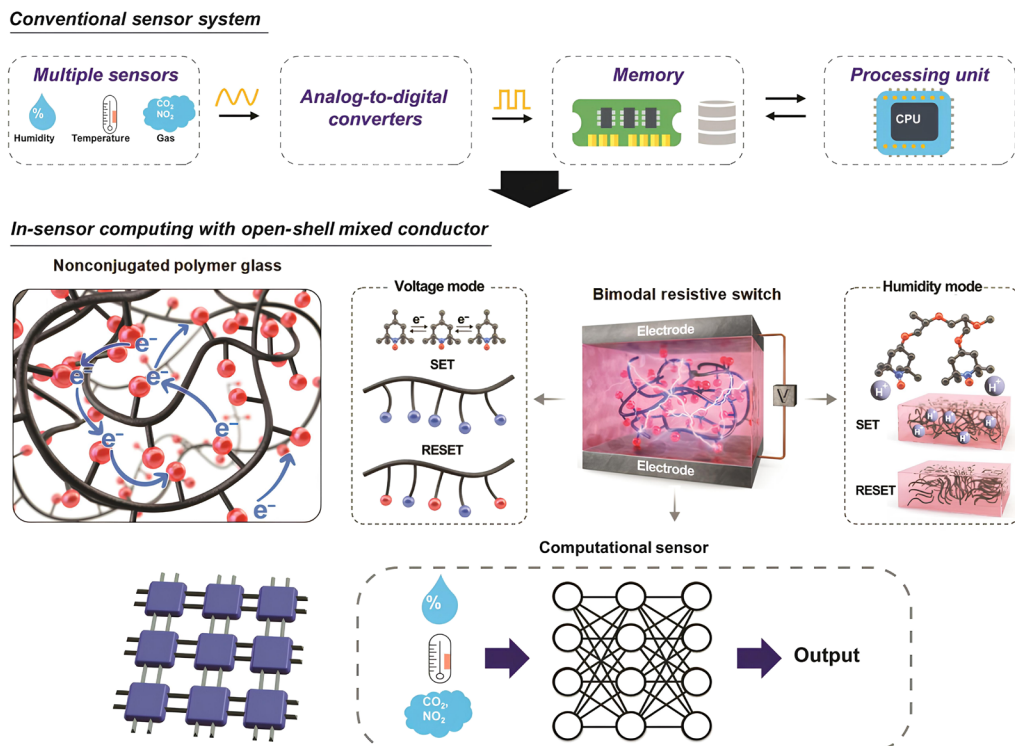


**Fig. 1. Overview of a nonconjugated radical polymer in multimodal device operation.** A model radical polymer transports charges through redox hopping between pendant radicals. In addition, it displays ionic conductivity owing to ionic moieties in the backbone (not shown for clarity). These features of the radical polymer enable bimodal resistive switching that is cooperatively operable by multiple inputs. The multimodal memristivity can be expanded to a humidity-dependent in-sensor computing system, with substantial advantages over conventional sensor systems. CPU, central processing unit.

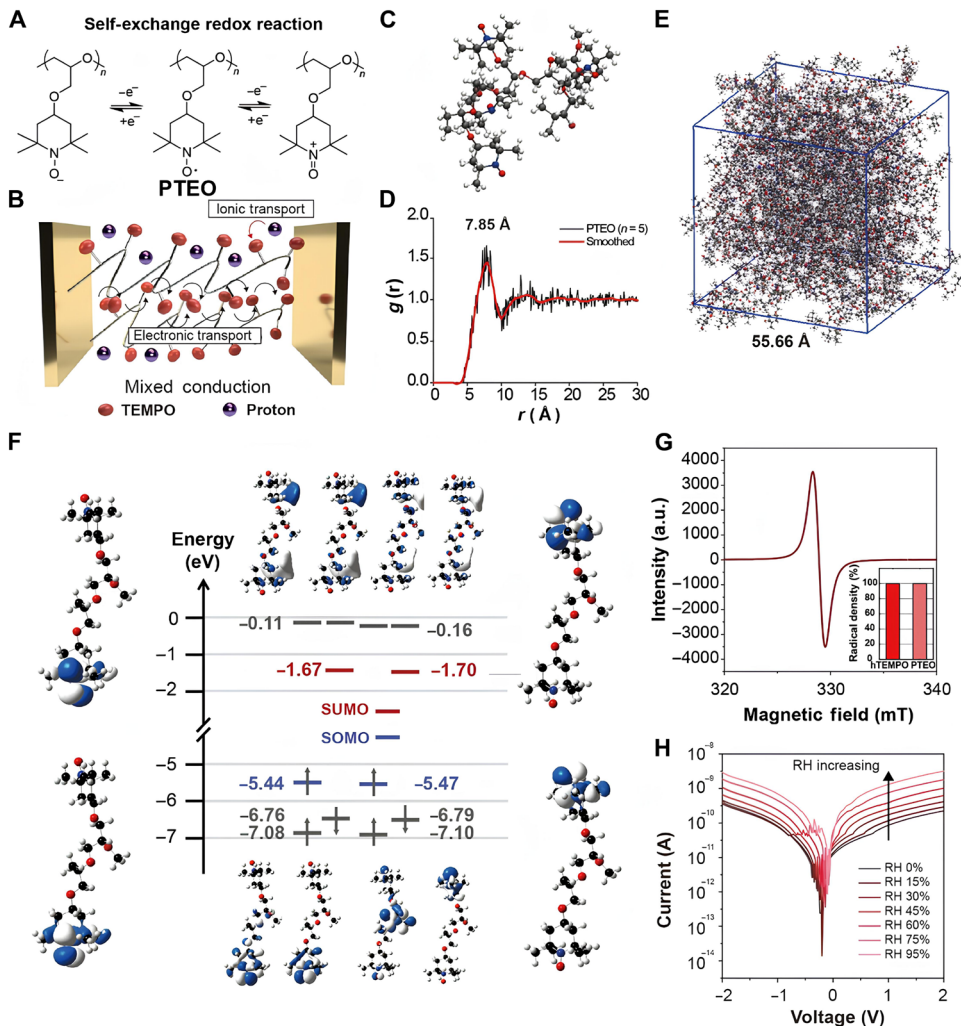


**Fig. 2. Characteristics of PTEO used in this study.** (A) Self-exchange redox reaction of PTEO. (B) Schematic illustration of mixed conduction in PTEO. In the illustration, the pendant radicals (red spheres) connected to the polymeric backbone (black) transport charges through consecutive hopping events, possibly interacting with ionic species (blue spheres) in the environment. (C) Optimized molecular structure of pentameric PTEO from MD simulation. (D) RDF calculated for nitrogen (N) atoms within each molecule. (E) Stabilized structure composed of 100 PTEO molecules obtained after 1 ns of the simulation. (F) DFT calculation of frontier energy levels for a dimeric PTEO. (G) ESR spectrum of PTEO. Inset displays the radical content of the PTEO as compared with a reference small-molecule TEMPO, 4-hydroxy TEMPO (hTEMPO). a.u., arbitrary units. (H) Solid-state  $I$ - $V$  curves of the PTEO and its humidity response.

molecular structure (Fig. 2C) revealed a radical proximity of ~6 to 8 Å (Fig. 2D), closely matching the proximity requirement for effective charge transport in small-molecule TEMPO derivatives (21, 29–31). In addition, density functional theory (DFT) calculations on a dimeric PTEO showed that the frontier molecular orbitals, including the singly occupied (SOMO) and singly unoccupied molecular orbitals (SUMO), are well localized within each TEMPO pendant unit (Fig. 2F and fig. S5). Notably, the electronic energy levels of the PTEO monomer remained virtually unaffected by chain extension, emphasizing the nonconjugated nature of the PTEO.

The differential scanning calorimetry (DSC) of the PTEO exhibits a near-room temperature glass transition temperature ( $T_g$ ), which can be further adjusted on demand through appropriate molecular weight engineering (fig. S6). The polymer displays considerable ambient stability, as revealed by corresponding electron spin resonance (ESR) analysis (Fig. 2G). In particular, the radical content

of the as-prepared PTEO was comparable to a small-molecule nitroxide (4-hydroxy TEMPO) as a reference based on the quantitative analysis (Fig. 2G, inset). Figure 2H demonstrates typical current-voltage ( $I$ - $V$ ) curves of the PTEO in a long-channel device (channel length, 80 μm) under a systematic control over relative humidity (RH). The humidity-dependent increase in the proton conductivity is a widely recognized phenomenon in poly(ethylene oxide) and the derivatives (32, 33), where the presence of ethylene oxides in the main chain facilitates the ionic conduction. In our case, the same ethylene oxide functionality in the backbone of the PTEO (Fig. 2A) provides the ion solubility (18), leading to the systematic increase in the proton conductivity as  $RH$  increases. The ionic nature of the conductivity was further confirmed by the characteristic time-dependent decay of the initial current into the steady-state current (related discussion provided below). The general characteristics of the PTEO in our study illustrate the robust nature of the radical

polymer as an organic memristive material, indicating its opportunities toward multimodal device operations.

### A radical polymer-based resistive switching

The concept of small-molecule radicals being memristive has been reported by Lee *et al.* (20), where a small-molecule nitronyl nitroxide displayed redox bistability for resistive switching. Although it exhibited notable cycling performance, the retention characteristics were only moderate ( $<10^3$  s), possibly due to limited ambient stability of nitronyl nitroxide (20). Alternatively, Yonekuta *et al.* (34) reported a battery-inspired multicomponent memory in 2007 through careful molecular orbital engineering and combination of nitroxide- and galvinoxyl-based macromolecules. In comparison, our demonstration represents a stable radical polymer inherently capable of resistive switching operation as a single component active layer, with highly reliable performance. Specifically, we envisioned that the intrinsic redox bistability and the polymeric nature of PTEO can serve as the basis of high-performance resistive switching operation. In addition, we emphasize that the exceptional ambient stability and processability of PTEO, both attributes benefiting from its (amorphous) polymeric nature, realize a marked enhancement in the device stability of the PTEO-based resistive switching.

Given the stable mixed conductivity (i.e., both ionic and electronic conductivity) of PTEO, we constructed MIM devices using PTEO as an active layer. The devices were fabricated using different electrode materials and the device architectures; both dot arrays and crossbars with either Au(bottom)/Cu(top) or Au/Au combinations of electrodes were used (namely, Au/PTEO/Cu and Au/PTEO/Au; Fig. 3A). Here, the thickness of the active layer was 100 nm, where device areas of  $50 \times 50 \mu\text{m}^2$ ,  $80 \times 80 \mu\text{m}^2$ , and  $100 \times 100 \mu\text{m}^2$  were tested, respectively. Figure 3 (B and C) summarizes the typical *I-V* sweep of Au/PTEO/Cu and Au/PTEO/Au devices, respectively (detailed experimental setup in fig. S7). The measurement was carried out with a voltage sweeping mode under ambient conditions (further measurement details are described in the Supplementary Materials). Both Au/PTEO/Cu and Au/PTEO/Au devices exhibited characteristic *I-V* curves indicative of a bipolar resistive switching; they were characterized by a clear distinction between a high resistance state (HRS) and a low resistance state (LRS), an abrupt transition between them, and a reversal of polarity between the SET and RESET processes. The dc voltage sweep was highly reliable and repeatable, with the voltages for SET and RESET ( $V_{\text{SET}}$  and  $V_{\text{RESET}}$ ) observed at 1.45 V ( $\pm 0.5$  V) and -0.6 V ( $\pm 0.14$  V) for the Au/PTEO/Cu device, respectively. Notably,  $V_{\text{SET}}$  and  $V_{\text{RESET}}$  for the Au/PTEO/Au were at 1.25 V ( $\pm 0.25$  V) and -0.59 V ( $\pm 0.14$  V), respectively, which matched closely with those of the Au/PTEO/Cu device. Furthermore, both devices displayed remarkable stability as revealed by the retention and cycling performance. Specifically, the devices exhibited  $>10^5$  s of retention (Fig. 3D) while displaying stable device performance after  $>250$  dc sweep cycles (Fig. 3E). In addition, the device exhibited remarkable long-term stability, which maintained its stable switching performance after 6 months of ambient storage (fig. S8). Overall, Fig. 3 (A to E) illustrates that our synthesized PTEO inherently exhibits resistive switching characteristics, corroborated by the observation that (i) the devices demonstrate independence from the nature of the electrode materials (vide supra) and (ii) the inertness of the gold electrode generally precludes the reversible formation of metallic filaments (20, 35).

To elucidate the conduction mechanism associated with the observed switching behavior, double logarithmic *I-V* curves were plotted (Fig. 3, F and G). Initially, in the HRS of our device, we observed a characteristic electrical behavior describing conduction through a polymer matrix, namely, trap-controlled space charge-limited conduction (SCLC) (Fig. 3G) (36, 37). Specifically, three distinct regions of charge conduction were observed: (i) ohmic conduction ( $I \propto V$ ), (ii) square law dependence ( $I \propto V^2$ ), and (iii) steep current increasing regions ( $I \propto V^\alpha$  with  $\alpha > 2$ ). It is noteworthy that the LRS of the device showed a comparable SCLC behavior, in contrast to the conducting filament type memristors, which typically exhibit ohmic conduction behavior across the entire LRS region (Fig. 3F). In addition, the conduction mechanism was apparently independent of the nature of the electrode materials, at both the LRS and the HRS (Fig. 3H and fig. S9). Last, to ascertain the origin of the bistability observed in the *I-V* measurements, cyclic voltammetry (CV) was conducted. Figure 3I presents a typical voltammogram of 0.1 mM PTEO in acetonitrile in the presence of an organic salt, tetrabutylammonium hexafluorophosphate. The voltammogram is in close agreement with those of small-molecule nitroxides described in the literature, exhibiting reversible and stable redox kinetics in a given voltage window (38). Specifically, the oxidation couples were observed at 0.75 V (versus Ag/AgCl), while the reduction couples occurred at -0.8 V (versus Ag/AgCl) (38). Overall, the mechanistic studies combined with electrochemical measurements confirm the origin of resistive bistability of PTEO conducive to stable switching operations.

Although the evidence strongly suggests SCLC in the LRS (thus ruling out the metallic filaments formation), revealing physical changes associated with the switching events is worthwhile. For this purpose, we have further analyzed the conduction mechanism from a different perspective, determining if it is characterized by interface or localized resistive switching (37). Figure S10 illustrates the cell area dependence of the LRS and HRS currents, demonstrating a relatively weak resistance dependence on the device area in the LRS; this characteristic indicates that the high conductance in the LRS is primarily associated with the formation of a localized conducting network. Considering that resistive switching occurs regardless of the type of the metal electrode (Fig. 3, B and C), it can be concluded that the switching mechanism in PTEO-based devices is the formation of nonmetallic, localized conductive network, driven by electrochemical changes between charged states of pendant radicals. Specifically, we propose that the applied electric field during the operation shifts the equilibrium between the redox states, leading to the profound changes in the conductivity (Fig. 3I).

As PTEO features its nonconjugated nature, more direct comparison on its switching behavior to that of the conjugated systems may provide additional insights. Memristive devices based on conjugated polymers have widely been reported, with various working principles including charge transfer (39, 40), space charge and traps (41), filamentary conduction (42), and other material-specific ones (43). Specifically, donor-acceptor conjugated polymers have been popular, which operate under the charge transfer and/or the trap filling models (44, 45). Electrically, the high conductance state (i.e., the LRS) of these memristive devices are often described by the ohmic conduction, which reflects the charge transfer or the trap-filled states that enable efficient charge transport within these materials. In contrast, the PTEO-based memristive device uniquely features the SCLC behavior at the LRS. It indicates that the change in its redox state during the device operation is directly ascribable to

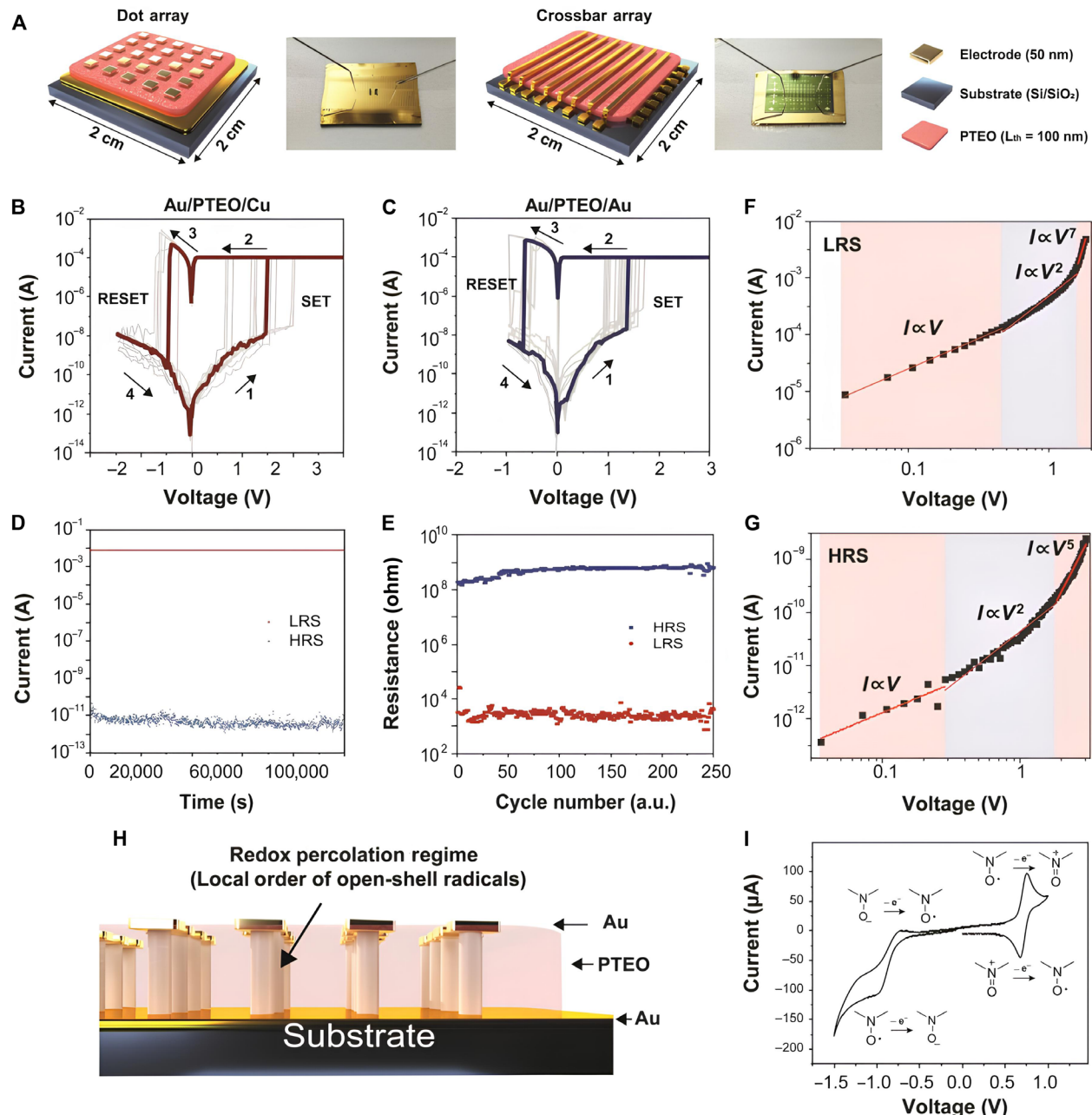


**Fig. 3. Device characteristics of PTEO-based resistive switching.** (A) Device architecture including dot arrays and crossbars, with electrode materials of either gold (bottom) or copper (top). (B and C)  $I$ - $V$  curves showing stable resistive switching of the (B) Au/PTEO/Cu device and (C) Au/PTEO/Au device. (D) Device stability test showing retention characteristics of PTEO-based resistive switching and (E) the cycling performance. (F and G) Mechanistic aspects of the PTEO-based resistive switching device. Double logarithmic  $I$ - $V$  curves of (F) HRS and (G) LRS. (H) Illustration of the conductive channel formation at the LRS due to the compositional change in pendent radical species in response to the applied voltage. (I) Cyclic voltammogram of PTEO displaying reversible redox kinetics upon variable voltages.

the formation of a distinct conductance state with a different trap state. While the trap-filling behavior within each conductance state may affect the inter-state transition, the observed SCLC behavior at the LRS strongly corroborates the intrinsic nature of the resistive switching pertaining to the PTEO-based device.

#### Bimodal resistive switching of the radical polymer

Building on the stable switching performance observed in the PTEO-based device, now, we explore its bimodal resistive switching

to seek the possibility toward effectively emulating the signal transduction in biological systems. We specifically examine the impact of the proton (as controlled by  $RH$ ) on the switching behavior, in which the proton represents a biological neurotransmitter. The concept of resistive bimodality was recently highlighted with different types of input variables, such as light and humidity (10, 46). Among these, a recent work by Song *et al.* (10) on a peptide-based memristor for neuromorphics is noteworthy. In their contribution, proton-coupled redox mediation in a peptide material was used for the

formation of metallic filament in its memristive operation (10). In contrast, our demonstration here features the bimodality and ion-electron cooperativity as an intrinsic material property, which neither relies on an external source of resistive components (e.g., metallic filament) nor acts merely as a resistive mediator.

It is worthwhile to consider the overarching influence of the proton on the resistive switching behavior of the PTEO-based memristive device. Specifically, we focus on the proton-coupled electron transfer (PCET) among its pendant radicals (i.e., TEMPO). PCET involving radical molecules, such as tyrosine and TEMPO derivatives, has widely been recognized with established in-depth mechanistic studies (47–49). In particular, it typically involves a hydrogenated TEMPO derivative, TEMPO hydroxylamine (TEMPOH; fig. S11) (50). The following pseudo self-exchange is thermodynamically favorable, which allows PCET throughout the polymer matrix (51)



In addition, the following equilibrium should be considered for the PTEO-based devices under the influence of humidity



While the latter equilibrium strongly favors the hydroxylamine form of TEMPO, the nitroxide (TEMPO $\cdot$ ) can readily be regenerated electrochemically during the device operation (52, 53). Notably, the TEMPOH has a much narrower redox potential window than that of TEMPO (53).

To investigate the experimental evidence on the TEMPOH species, we conducted time-dependent ultraviolet-visible (UV-Vis) spectroscopy analysis on a solid film of PTEO (54). We found that the elevated level of humidity resulted in the generation of the TEMPOH species within the polymer matrix, as revealed by the systematic decrease in the apparent extinction coefficient ( $\epsilon$ ) at the absorption maximum (~460 nm) with the time evolution (fig. S12). This attributed to the characteristic extinct coefficient of TEMPOH compared to that of TEMPO $^+$  ( $20.0 \text{ M}^{-1} \text{ cm}^{-1}$  at 459 nm) and TEMPO $\cdot$  ( $10.5 \text{ M}^{-1} \text{ cm}^{-1}$  at 459 nm), which is only negligible (54). Noteworthy is that the formation of TEMPOH was limited to a minority as compared to the corresponding nitroxide, likely due to the limited amounts of available protons within the solid-state setup. In addition, the kinetic isotope effect associated with (i) the proton conduction and (ii) the PCET was further assessed to elucidate the active involvement of protons in these processes (fig. S13). Overall, the generation of TEMPOH at elevated humidity and the possible equilibria shifts associated with it are expected to substantially affect the resultant resistive switching behavior. This is substantiated by the localized nature of the conductive network formation in PTEO-based resistive switching as discussed above, which should be sensitive to a minute change in the compositional change among the variable redox states of the PTEO. Specifically, the involvement of the hydroxylamine at elevated humidity affects the switching behavior of PTEO-based devices by (i) providing an additional conductance state with markedly reduced operation voltage and (ii) affecting the preexisting equilibria among the TEMPO $^+$ , TEMPO $\cdot$ , and TEMPO $^-$  species established under ambient conditions.

Building on this, we recorded changes in the  $V_{\text{SET}}$  corresponding to the systematic variation in the proton concentration in our PTEO-based memristive device (Fig. 4, A and B). We noted a notable shift in  $V_{\text{SET}}$  when  $RH$  was increased from 20 to 60%; specifically,  $V_{\text{SET}}$  systematically decreased from >7 V at an  $RH$  of 20%,

whereas it was shifted to 3 V at 40%  $RH$  and eventually to ~2 V at an  $RH$  of 60%. Following this observation, we conducted further tests on the device operation, emulating the concerted activation processes in neuronal synapses (Fig. 4C). Specifically, we applied programmed humidity pulses to the device, ranging from 5 to 95%  $RH$ , at a fixed read voltage ( $V_{\text{read}}$ ) of 0.3 V throughout the  $RH$  sweep. The device exhibited distinct SET and RESET behaviors in response to the changes in the proton concentration, with the SET operation occurring at ~90%  $RH$  and the RESET at 7%  $RH$ . The device demonstrated excellent stability over exposure to the humid environment, maintaining the retention time exceeding  $10^4$  s for both the LRS and the HRS (Fig. 4D). Moreover, we were able to reproduce the complementary interplay between neurotransmitters in their signal transduction. Specifically, we applied programmed pulses as illustrated in Fig. 4E, which were associated with distinct SET and RESET operations by voltage and humidity, respectively. The SET operation enabled by the proton accumulation was disabled by the applied voltage pulse, which is reminiscent of the dynamic interplay between the neurotransmitters. Overall, our demonstration of bimodality in PTEO-based devices signifies the cooperative resistive switching that is intrinsic, making it suitable for advance biorealistic neuromorphic systems.

### A radical polymer-based in-sensor computing system

Building on the intrinsic memristivity and proton conductivity of PTEO, last, we demonstrate a humidity-dependent in-sensor computing system (Fig. 5). Briefly, conventional sensor systems have suffered from massive data transfers between components, namely, the sensor, converter, and processing units. This has resulted in notable delays and power consumption and necessity for analog-to-digital converters. These converters are critical for transforming analog sensory data into digital ones to facilitate processing tasks; however, they are notoriously laborious in terms of both time and power consumption. Conversely, an in-sensor computing system can substantially alleviate the limitations of the traditional one by executing computational operations directly on the sensory device. Within this context, memristive devices feature adjustable resistive switching with nonvolatility, offering opportunities for energy-efficient vector-matrix multiplications (e.g., dot products) in an array architecture (55–57). As hardware-implemented memristive neuromorphic computing can efficiently process deep learning to find hidden correlations and patterns, a memristive device with sensory functions is suitable for the practical implementation of the in-sensor computing system. As a demonstration of our concept, we built an in-sensor computing system for accurate  $RH$  sensing by adapting the PTEO-based memristive device developed in this study.

A typical electrical characteristic of the PTEO-based memristive device indicates that the ionic nature of the proton conduction displays characteristic decay of the initial current into the steady-state current (Fig. 5A). Specifically, it was confirmed that the current decay ( $\Delta I$ ) after 30 s has distinct features depending on  $RH$ , verified across different batches; this is possibly due to the dynamic nonlinear response of PTEO functionality in response to  $RH$  values (Fig. 5, B and C). Therefore, the initial current and the current decay after 30 s of the PTEO-based memistor were used as input features. Note that the input values at the LRS of the resistive switching were also available for this purpose, as revealed by the dependence of the LRS current on the humidity (fig. S14). To demonstrate the feasibility of in-sensor computing applications, we conducted a device-to-system

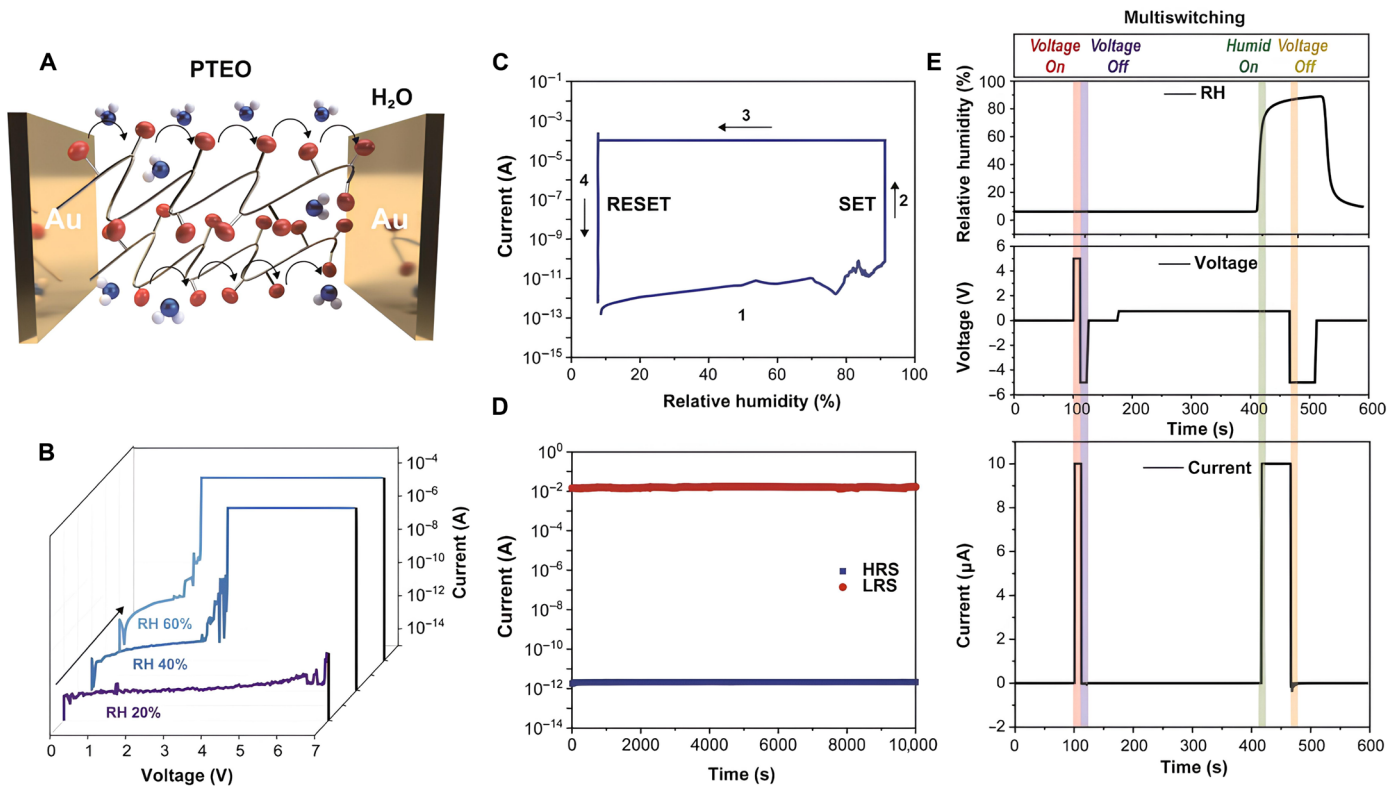


**Fig. 4. Humidity response and bimodal operation of PTEO-based resistive switching.** (A) Schematic illustration of the PTEO device under a humid environment. (B) Humidity-dependent SET behavior, (C) I-V curve, and (D) retention characteristics of PTEO-based resistive switching under humidity exposure. (E) Bimodal operation of PTEO-based resistive switching displaying SET/RESET behaviors at both stimuli.

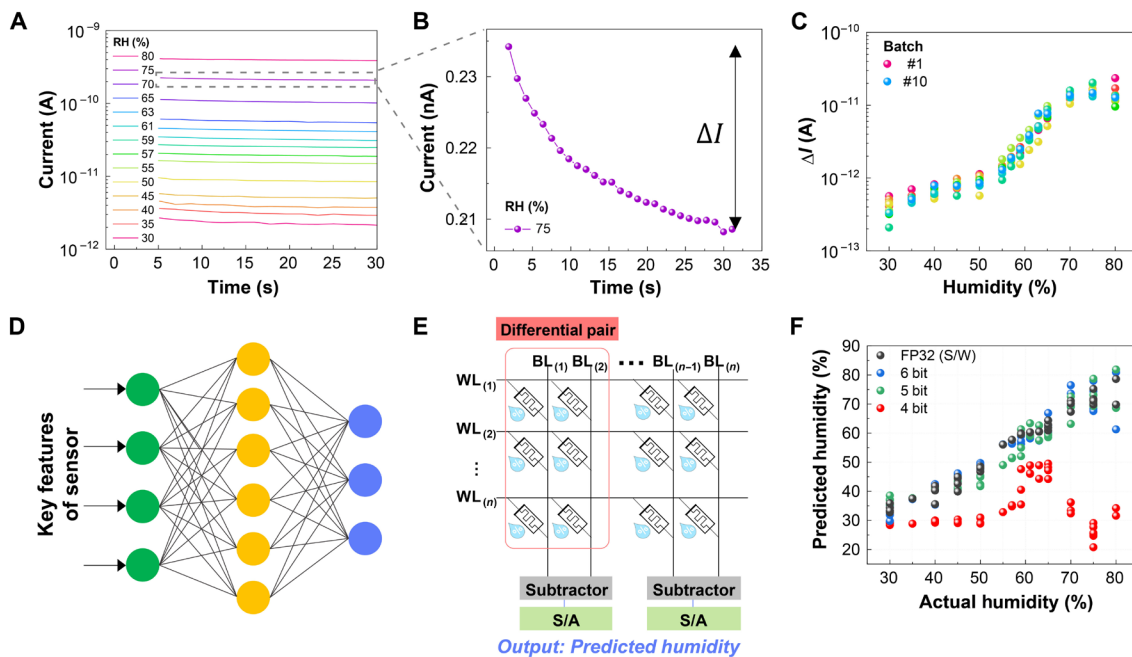


**Fig. 5. In-sensor computing system for RH sensing.** (A) Humidity-dependent current characteristics over time. (B) Current decaying feature as a function of the elapsed time. (C) Current decay after 30 s depending on RH for different 10 batches. (D) Artificial neural network for the regression task. (E) Block diagram for the circuit of the memristive neural network. WL, word line; BL, bit line; S/A, sense amplifier. (F) Performance of the memristive neural network for the in-sensor computing-based regression task. In the legend, "S/W" stands for the software, indicating the software-based 32-bit floating point.

simulation for performing a regression model. This simulation used a supervised learning-based artificial neural network with a three-layer architecture, including the 2 inputs and 20 hidden neurons, to predict the *RH* accurately (Fig. 5D). The inputs, when applied to the neural network, underwent vector matrix multiplication after being weighted and summed across synapse layers. Figure 5E exhibits the block diagram for implementing the memristive neural network, where two memristor devices were paired to represent positive and negative weight values by subtracting the conductance of the synapse with a negative value from that with a positive value. Figure 5F shows the performance of the memristive neural network for an in-sensor computing-based regression task, indicating that synapse weights over 5 bit provide performance comparable to a software-based 32-bit floating point (FP32). The PTEO-based memristive device is capable of implementing both 5-bit and 6-bit configurations due to its high on/off ratio of  $10^6$ ; however, as the number of bits increases, the read disturbance and retention characteristics deteriorate. Therefore, a 5-bit configuration is recommended for accurate *RH* prediction with minimal data features. Overall, these results strongly indicate that the PTEO-based memristive device is capable of representing advanced biorealistic systems and performing in-sensor computing operation, all within practicality of the material property inherent to the radical polymer.

## DISCUSSION

In this work, we demonstrated intrinsic multimodal memristivity of a nonconjugated radical polymer. The radical polymer-based resistive switching device exhibited stable performance across retention tests and iterative cycling due to its stable redox kinetics and ambient stability. We leveraged the proton accumulation in the radical polymer to represent an advanced biorealistic system, wherein the cooperative and complementary interplay between neurotransmitters was reproduced. We further expanded our system toward humidity-dependent in-sensor computing operation, showcasing the immediate and practical applications of the radical polymer.

By doing so, our contribution demonstrated a material system capable of realizing important aspects of biological systems as well as a material platform displaying multimodal memristivity. In addition, we provided an exemplary case of an unconventional organic conductor system, which features distinct advantages in its material property over that of the existing materials. As a result, our work finds its significance in promoting the understanding toward complex interplay that occurs in biological systems and providing the strategies to effectively reproduce these systems. In addition, our work greatly expands the materials library for the future memristive devices.

Although our work signifies an important step toward an innovative device platform for next-generation information technologies, further efforts are needed before its practical implementation. First, while the initial evidence of multimodal memristivity within the material platform was provided, an explicit demonstration of the synaptic plasticity has yet to be shown. A study on a more complete description of various types of synaptic plasticity is currently ongoing. Second, although we have investigated aspects of the resistive switching behavior pertaining to the radical polymer, more direct and explicit evidence on its origin should be valuable. Advanced characterization tools, such as in operando techniques, may shed light on the fundamental nature of the switching and related phenomena.

## MATERIALS AND METHODS

### Materials

All the chemicals were purchased from commercial sources and used without further purification. These include 4-glycidyloxy TEMPO (>95%, TCI), 18-crown-6 (99%, Sigma-Aldrich), diglyme (99%), potassium *tert*-butoxide (*t*-BuOK; >98%, Sigma-Aldrich), tetrahydrofuran (THF; >99.9%, Sigma-Aldrich), chloroform (>99%, Sigma-Aldrich), acetonitrile (99.8%, Sigma-Aldrich), tetrabutylammonium hexafluorophosphate (>98%, TCI), deuterium oxide (99.9%, Sigma-Aldrich), and phenylhydrazine (97%, Sigma-Aldrich).

### Synthesis of PTEO

The synthesis of PTEO followed our previous work. Briefly, to a solution of 4-glycidyloxy TEMPO (300 mg, 1.31 mmol) and 18-crown-6 (48 mg, 0.18 mmol) in diglyme (0.2 ml) was added 1 M *t*-BuOK solution in THF (61  $\mu$ l, 0.061 mmol) under argon atmosphere. The mixture was stirred at 40°C for 20 hours. The resulting viscous mixture was dissolved in chloroform and slowly poured into hexane. The precipitate was collected by centrifugation and dried under vacuum at room temperature to yield PTEO as a red solid.

### MD simulation

We used the general AMBER force field within the GROMACS 2022 package. A simulation model comprising 100 PTEO ( $n = 5$ ) molecules, totaling 19,800 atoms, was generated. An MD simulation was conducted for 1 ns with a time step of 0.1 fs under the isothermal-isobaric (NPT) ensemble. The system was maintained at a constant pressure of 1 atm using the Parrinello-Rahman barostat, while the temperature was held at 25°C via the Berendsen thermostat. Non-bonding interactions were updated every 1 fs within a cutoff sphere of 1.2 nm. Electrostatic interactions were computed using the particle mesh Ewald algorithm, using a space cutoff of 0.9 nm and a Fourier grid spacing of 0.09 nm. Following the MD simulation, the radial distribution function (RDF) between the nitrogen (N) atoms within PTEO molecules was calculated.

### DFT calculation

Geometry optimizations of PTEO with open-shell electron configurations were carried out in the gas phase using Gaussian 16 quantum-chemical calculation software with UB3LYP functional and 6-31g+(d,p) basis set. Vibrational frequency calculations were performed at the same level to confirm the stable minima.

### Sample preparation

For the general purpose of device fabrication, a designated amount of PTEO was dissolved in acetonitrile, which was filtered twice with a syringe filter (0.2  $\mu$ m, 13 mm, Whatman). UV-Vis spectroscopy analysis was performed either on the solution or the solid film of PTEO. The solution was prepared to a designated concentration in chloroform, which was transferred to a quartz cell with a path length of 10 mm. The measurement of the solid film was carried out with a thin film of PTEO on a quartz cell wall, which was placed in a sample chamber with controllable humidity. Electrochemical measurements were carried out for a 0.1 mM acetonitrile solution of PTEO, with 0.1 M tetrabutylammonium hexafluorophosphate as an electrolyte. For ESR measurements, each sample was dissolved in acetone to give a molar concentration of 0.1 mM. A commercial ESR tube container with an effective sample volume of 130  $\mu$ l was used.

## Device fabrication

For a general process of device fabrication, a 2 cm × 2 cm of thermal oxide (oxide thickness, 300 Å) was thoroughly rinsed with a standard protocol using acetone, isopropyl alcohol, and deionized water using bath sonication (JAC-3010, Kodo, Japan). The electrodes were deposited by thermal evaporation of either gold or copper sources to the thickness of 40 nm using shadow masks. The active layer of PTEO was spun coat (Won Corporation, South Korea) to achieve the layer thickness of 100 nm.

## Characterization

Absorption spectra were recorded with a multipurpose UV–Vis–NIR (near-infrared) spectrometer (V-670, Jasco, Japan) in a dual-beam setup. NMR spectra of PTEO were recorded on a 600-MHz spectrometer (ProPulse, Agilent, United States) with tetramethylsilane as an internal standard. DSC analysis was carried out using a simultaneous DSC–TGA (thermogravimetric analysis) analyzer (STDQ-600, TA Instruments, United States). The DSC cycle includes heating up ( $10^{\circ}\text{C min}^{-1}$ ) of the sample to  $90^{\circ}\text{C}$  and cooling down to  $-50^{\circ}\text{C}$  with 10 min of isothermal steps under nitrogen atmosphere. The second scan was recorded and used for the plotting. For the electrical measurements, a multipurpose parameter analyzer (Keithley-4200 SCS, Tektronix, United States) equipped with pre-amplifier (4225-RPM, Tektronix, United States) was used. A dedicated probe tip (tip diameter of 0.4 μm, Modusys, South Korea) was used for the analysis of the dot arrays. Electrochemical analysis was carried out on an electrochemical workstation (Gamry Instruments, United States). The voltammogram was obtained at a scan rate of  $10 \text{ mV s}^{-1}$ . ESR measurements were carried out with an electron paramagnetic resonance spectrometer (JES-FA100, JEOL). All the measurements were carried out at room temperature. A solution of 4-hydroxy TEMPO was used as an external reference. Experimental parameters are as follows: microwave frequency, 9.226 GHz; microwave power, 0.998 mW; modulation amplitude, 1 mT; modulation frequency, 100 kHz; time constant, 0.03 s.

## Bimodal resistive switching

For the precise control of  $RH$ , a multipurpose gas sensing measurement system (Phocos, South Korea) was used.  $RH$  sweep was carried out on a programmed input of either an argon gas or a water vapor, where the maximum flow rate was fixed at 500 standard cubic centimeter per minute. All the electrical measurements at variable  $RH$  were carried out in a dedicated sealed chamber. For the isotope effect analysis, the same gas sensing system with a  $\text{D}_2\text{O}$  reservoir was used. For the switching between  $RH$  and relative deuterium oxide concentration ( $RD$ ) modes, we carried out at least 1 hour of equilibration cycle before each measurement.

## Device-to-system level simulation for in-sensor computing operation

Measurements of the input data for the in-sensor computing operation were conducted on a PTEO device of intentionally elongated channel length (80 μm) to prevent possible switching up. To enhance the resolution between each data, the read voltage was increased to 5 V. Humidity was controlled on a programmed input of  $RH$  series, varying from 30 to 80%. The interval was set to 2% in the  $RH$  range of 55 to 65% and 5% otherwise. For the device-to-system level simulation, we designed a three-layer artificial neural network system for a regression model. We assumed that the PTEO devices

were configured in the form of a crossbar array architecture to implement the simulation. Using the initial current and current decay after 30 s of the PTEO devices as input features and the corresponding humidity as a label, a dataset was constructed. With the dataset, we conducted the learning of the synaptic weights through software-based back propagation process (Python). The synaptic weights were quantized based on the conductance bit of the device. In this simulation, the quantized synaptic weights were mapped to the crossbar array, which enabled a vector-matrix product by Kirchhoff's and Ohm's laws. Regression models were implemented using a crossbar array composed of PTEO devices, which solely performed the inference operations. This eliminated the need for supplementary processing units to predict  $RH$ , indicating in-sensor computing operation.

## Supplementary Materials

This PDF file includes:

Figs. S1 to S14

## REFERENCES AND NOTES

- J. J. Yang, D. B. Strukov, D. R. Stewart, Memristive devices for computing. *Nat. Nanotechnol.* **8**, 13–24 (2013).
- M. K. Song, J. H. Kang, X. Zhang, W. Ji, A. Ascoli, I. Messaris, A. S. Demirkol, B. Dong, S. Agarwal, W. Wan, S. M. Hong, S. G. Cardwell, I. Boybat, J. S. Seo, J. S. Lee, M. Lanza, H. Yeon, M. Onen, J. Li, B. Yildiz, J. A. del Alamo, S. Kim, S. Choi, G. Milano, C. Ricciardi, L. Alif, Y. Chai, Z. Wang, H. Bhaskaran, M. C. Hersam, D. Strukov, H. S. P. Wong, I. Valov, B. Gao, H. Wu, R. Tetzlaff, A. Sebastian, W. Lu, L. Chua, J. J. Yang, J. Kim, Recent advances and future prospects for memristive materials, devices, and systems. *ACS Nano* **17**, 11994–12039 (2023).
- C. Du, W. Ma, T. Chang, P. Sheridan, W. D. Lu, Biorealistic implementation of synaptic functions with oxide memristors through internal ionic dynamics. *Adv. Funct. Mater.* **25**, 4290–4299 (2015).
- M. Prezioso, F. Merrikh-Bayat, B. D. Hoskins, G. C. Adam, K. K. Likharev, D. B. Strukov, Training and operation of an integrated neuromorphic network based on metal-oxide memristors. *Nature* **521**, 61–64 (2015).
- Y. van de Burgt, A. Melianas, S. T. Keene, G. Malliaras, A. Salleo, Organic electronics for neuromorphic computing. *Nat. Electron.* **1**, 386–397 (2018).
- L. Yuan, S. Liu, W. Chen, F. Fan, G. Liu, Organic memory and memristors: From mechanisms, materials to devices. *Adv. Electron. Mater.* **7**, 2100432 (2021).
- S. Goswami, S. Goswami, T. Venkatesan, An organic approach to low energy memory and brain inspired electronics. *Appl. Phys. Rev.* **7**, 021303 (2020).
- S. Gao, X. Yi, J. Shang, G. Liu, R. W. Li, Organic and hybrid resistive switching materials and devices. *Chem. Soc. Rev.* **48**, 1531–1565 (2019).
- A. Gumusengen, A. Melianas, S. T. Keene, A. Salleo, Materials strategies for organic neuromorphic devices. *Annu. Rev. Mat. Res.* **51**, 47–71 (2021).
- M. K. Song, S. D. Namgung, D. Choi, H. Kim, H. Seo, M. Ju, Y. H. Lee, T. Sung, Y. S. Lee, K. T. Nam, J. Y. Kwon, Proton-enabled activation of peptide materials for biological bimodal memory. *Nat. Commun.* **11**, 5896 (2020).
- E. O. Neftci, B. B. Averbeck, Reinforcement learning in artificial and biological systems. *Nat. Mach. Intell.* **1**, 133–143 (2019).
- J. Du, L. R. Reznikov, M. P. Price, X.-M. Zha, Y. Lu, T. O. Moninger, J. A. Wemmie, M. J. Welsh, Protons are a neurotransmitter that regulates synaptic plasticity in the lateral amygdala. *Proc. Natl. Acad. Sci. U.S.A.* **111**, 8961–8966 (2014).
- S. T. M. Tan, A. Gumusengen, T. J. Quill, G. S. LeCroy, G. E. Bonacchini, I. Denti, A. Salleo, Mixed ionic-electronic conduction, a multifunctional property in organic conductors. *Adv. Mater.* **34**, e2110406 (2022).
- N. A. Kukhta, A. Marks, C. K. Luscombe, Molecular design strategies toward improvement of charge injection and ionic conduction in organic mixed ionic-electronic conductors for organic electrochemical transistors. *Chem. Rev.* **122**, 4325–4355 (2022).
- C. J. Kousseff, R. Halaksa, Z. S. Parr, C. B. Nielsen, Mixed ionic and electronic conduction in small-molecule semiconductors. *Chem. Rev.* **122**, 4397–4419 (2022).
- J. Lutkenhaus, A radical advance for conducting polymers. *Science* **359**, 1334–1335 (2018).
- Y. Joo, V. Agarkar, S. H. Sung, B. M. Savoie, B. W. Boudouris, A nonconjugated radical polymer glass with high electrical conductivity. *Science* **359**, 1391–1395 (2018).
- I. Yu, D. Jeon, B. Boudouris, Y. Joo, Mixed ionic and electronic conduction in radical polymers. *Macromolecules* **53**, 4435–4441 (2020).

19. Y. Tan, S. N. Hsu, H. Tahir, L. Dou, B. M. Savoie, B. W. Boudouris, Electronic and spintronic open-shell macromolecules, quo vadis? *J. Am. Chem. Soc.* **144**, 626–647 (2022).
20. J. Lee, E. Lee, S. Kim, G. S. Bang, D. A. Shultz, R. D. Schmidt, M. D. E. Forbes, H. Lee, Nitronyl nitroxide radicals as organic memory elements with both n- and p-type properties. *Angew. Chem. Int. Ed.* **50**, 4414–4418 (2011).
21. Y. Tan, N. C. Casetti, B. W. Boudouris, B. M. Savoie, Molecular design features for charge transport in nonconjugated radical polymers. *J. Am. Chem. Soc.* **143**, 11994–12002 (2021).
22. M. E. Hay, S. Hui Wong, S. Mukherjee, B. W. Boudouris, Controlling open-shell loading in norbornene-based radical polymers modulates the solid-state charge transport exponentially. *J. Polym. Sci. B Polym. Phys.* **55**, 1516–1525 (2017).
23. A. G. Baradwaj, S. H. Wong, J. S. Lester, A. J. Wingate, M. E. Hay, B. W. Boudouris, Impact of the addition of redox-active salts on the charge transport ability of radical polymer thin films. *Macromolecules* **49**, 4784–4791 (2016).
24. L. Rostro, A. G. Baradwaj, B. W. Boudouris, Controlled radical polymerization and quantification of solid state electrical conductivities of macromolecules bearing pendant stable radical groups. *ACS Appl. Mater. Interfaces* **5**, 9896–9901 (2013).
25. K. Oyaizu, H. Nishide, Radical polymers for organic electronic devices: A radical departure from conjugated polymers? *Adv. Mater.* **21**, 2339–2344 (2009).
26. Y. Xie, K. Zhang, Y. Yamauchi, K. Oyaizu, Z. Jia, Nitroxide radical polymers for emerging plastic energy storage and organic electronics: Fundamentals, materials, and applications. *Mater. Horiz.* **8**, 803–829 (2021).
27. S. Akkiraju, J. Vergados, L. Hoagland, Z. Lu, V. Anandan, B. W. Boudouris, Design of mixed electron- and ion-conducting radical polymer-based blends. *Macromolecules* **54**, 5178–5186 (2021).
28. K. Sato, T. Sukegawa, K. Oyaizu, H. Nishide, Synthesis of poly(TEMPO-substituted glycidyl ether) by utilizing t-BuOK/18-crown-6 for an organic cathode-active material. *Macromol. Symp.* **351**, 90–96 (2015).
29. Z. Liang, S. N. Hsu, Y. Tan, H. Tahir, H. J. Kim, K. Liu, J. F. Stoehr, M. Zeller, L. Dou, B. M. Savoie, B. W. Boudouris, Significant charge transport effects due to subtle molecular changes in nitroxide radical single crystals. *Cell Rep. Phys. Sci.* **4**, 101409 (2023).
30. T. Ma, E. Fox, M. Qi, C. H. Li, K. A. N. Sachithani, K. Mohanty, D. P. Tabor, E. B. Pentzer, J. L. Lutkenhaus, Charge transfer in spatially defined organic radical polymers. *Chem. Mater.* **35**, 9346–9351 (2023).
31. Y. Tan, J. Li, S. Li, H. Yang, T. Chi, S. B. Shirling, K. Liu, B. M. Savoie, B. W. Boudouris, C. M. Schroeder, Enhanced electron transport in nonconjugated radical oligomers occurs by tunneling. *Nano Lett.* **23**, 5951–5958 (2023).
32. S. Patra, A. B. Puthirath, T. V. Vineesh, S. Narayanan, B. Soman, S. Suriyakumar, A. M. Stephan, T. N. Narayanan, On the development of a proton conducting solid polymer electrolyte using poly(ethylene oxide). *Sustain. Energy Fuels* **2**, 1870–1877 (2018).
33. N. Turetta, M. A. Stoeckel, R. Furlan de Oliveira, F. Devaux, A. Greco, C. Cendra, S. Gullace, M. Gicevičius, B. Chattopadhyay, J. Liu, G. Schweicher, H. Sirringhaus, A. Salleo, M. Bonn, E. H. G. Backus, Y. H. Geerts, P. Samori, High-performance humidity sensing in π-conjugated molecular assemblies through the engineering of electron/proton transport and device interfaces. *J. Am. Chem. Soc.* **144**, 2546–2555 (2022).
34. Y. Yonekuta, K. Susuki, K. Oyaizu, K. Honda, H. Nishide, Battery-inspired, nonvolatile, and rewritable memory architecture: A radical polymer-based organic device. *J. Am. Chem. Soc.* **129**, 14128–14129 (2007).
35. U. S. Bhansali, M. A. Khan, D. Cha, M. N. AlMadoun, R. Li, L. Chen, A. Amassian, I. N. Odeh, H. N. Alshareef, Metal-free, single-polymer device exhibits resistive memory effect. *ACS Nano* **7**, 10518–10524 (2013).
36. A. Rose, Space-charge-limited currents in solids. *Phys. Rev.* **97**, 1538–1544 (1955).
37. B. C. Jang, H. Seong, S. K. Kim, J. Y. Kim, B. J. Koo, J. Choi, S. Y. Yang, S. G. Im, S. Y. Choi, Flexible nonvolatile polymer memory array on plastic substrate via initiated chemical vapor deposition. *ACS Appl. Mater. Interfaces* **8**, 12951–12958 (2016).
38. L. Wylie, T. Blesch, R. Freeman, K. Hatakeyama-Sato, K. Oyaizu, M. Yoshizawa-Fujita, E. I. Izgorodina, Reversible reduction of the TEMPO radical: One step closer to an all-organic redox flow battery. *ACS Sustain. Chem. Eng.* **8**, 17988–17996 (2020).
39. C. J. Chen, H. J. Yen, W. C. Chen, G. S. Liou, Resistive switching non-volatile and volatile memory behavior of aromatic polyimides with various electron-withdrawing moieties. *J. Mater. Chem.* **22**, 14085–14093 (2012).
40. S. J. Liu, Z. H. Lin, Q. Zhao, Y. Ma, H. F. Shi, M. D. Yi, Q. D. Ling, Q. L. Fan, C. X. Zhu, E. T. Kang, W. Huang, Flash-memory effect for polyfluorenes with on-chain iridium(III) complexes. *Adv. Funct. Mater.* **21**, 979–985 (2011).
41. Y. C. Lai, K. Ohshimizu, W. Y. Lee, J. C. Hsu, T. Higashihara, M. Ueda, W. C. Chen, Electrically bistable memory devices based on all-conjugated block copolythiophenes and their PCBM composite films. *J. Mater. Chem.* **21**, 14502–14508 (2011).
42. Z. Wang, F. Zeng, J. Yang, C. Chen, F. Pan, Resistive switching induced by metallic filaments formation through poly(3,4-ethylene-dioxythiophene):poly(styrenesulfonate). *ACS Appl. Mater. Interfaces* **4**, 447–453 (2012).
43. F. Paul, S. Paul, To be or not to be—Review of electrical bistability mechanisms in polymer memory devices. *Small* **18**, e2106442 (2022).
44. W. Elsawy, M. Son, J. Jang, M. J. Kim, Y. Ji, T. W. Kim, H. C. Ko, A. Elbarbary, M. H. Ham, J. S. Lee, Isoindigo-based donor–acceptor conjugated polymers for air-stable nonvolatile memory devices. *ACS Macro Lett.* **4**, 322–326 (2015).
45. H. C. Wu, C. L. Liu, W. C. Chen, Donor–acceptor conjugated polymers of arylene vinylene with pendent phenanthro[9,10-d]imidazole for high-performance flexible resistor-type memory applications. *Polym. Chem.* **4**, 5261–5269 (2013).
46. X. Chen, K. Zeng, X. Zhu, G. Ding, T. Zou, C. Zhang, K. Zhou, Y. Zhou, S.-T. Han, Light driven active transition of switching modes in homogeneous oxides/graphene heterostructure. *Adv. Sci.* **6**, 1900213 (2019).
47. W. D. Morris, J. M. Mayer, Separating proton and electron transfer effects in three-component concerted proton-coupled electron transfer reactions. *J. Am. Chem. Soc.* **139**, 10312–10319 (2017).
48. J. W. Darcy, B. Koroniewicz, G. A. Parada, J. M. Mayer, A continuum of proton-coupled electron transfer reactivity. *Acc. Chem. Res.* **51**, 2391–2399 (2018).
49. L. Q. Nguyen, R. R. Knowles, Catalytic C–N bond-forming reactions enabled by proton-coupled electron transfer activation of amide N–H bonds. *ACS Catal.* **6**, 2894–2903 (2016).
50. H. Li, Y. H. Guo, J. Y. Wu, M. T. Zhang, Proton-coupled electron transfer oxidation of O–H bond by the N-radical cation of Wurster's blue salt (TMPDA<sup>+</sup>). *Chem. Commun.* **55**, 3465–3468 (2019).
51. A. Wu, E. A. Mader, A. Datta, D. A. Hrovat, W. T. Borden, J. M. Mayer, Nitroxyl radical plus hydroxylamine pseudo self-exchange reactions: Tunneling in hydrogen atom transfer. *J. Am. Chem. Soc.* **131**, 11985–11997 (2009).
52. O. Nolte, P. Rohland, N. Ueberschaar, M. D. Hager, U. S. Schubert, Stability of TMA-TEMPO-based aqueous electrolytes for redox-flow batteries. *J. Power Sources* **525**, 230996 (2022).
53. X. Zhao, J. D. Yang, J. P. Cheng, Revisiting the electrochemistry of TEMPOH analogues in acetonitrile. *J. Org. Chem.* **88**, 540–547 (2023).
54. J. B. Gerken, S. S. Stahl, High-potential electrocatalytic O<sub>2</sub> reduction with nitroxyl/NO<sub>x</sub> mediators: Implications for fuel cells and aerobic oxidation catalysis. *ACS Cent. Sci.* **1**, 234–243 (2015).
55. Z. Zhang, X. Zhao, X. Zhang, X. Hou, X. Ma, S. Tang, Y. Zhang, G. Xu, Q. Liu, S. Long, In-sensor reservoir computing system for latent fingerprint recognition with deep ultraviolet photo-synapses and memristor array. *Nat. Commun.* **13**, 6590 (2022).
56. P. Yao, H. Wu, B. Gao, J. Tang, Q. Zhang, W. Zhang, J. J. Yang, H. Qian, Fully hardware-implemented memristor convolutional neural network. *Nature* **577**, 641–646 (2020).
57. D. B. Strukov, G. S. Snider, D. R. Stewart, R. S. Williams, The missing memristor found. *Nature* **453**, 80–83 (2008).

**Acknowledgments**

**Funding:** This work was supported by the Korea Institute of Science and Technology (Korea) Institutional Program, National Research Foundation of Korea grant (RS-2023-00208313), National Research Foundation of Korea grant (2022K1A3A1A91093969), National Research Foundation of Korea grant (2021R1A2B5B03001416), National Research Foundation of Korea grant (2022R1C1C1006557), and National Research Foundation of Korea grant funded by the Korean government (MSIT) (no. 2021R1A2B5B03001416). **Author contributions:** Conceptualization: J.K., B.C.J., S.G.I., and Y.J. Methodology: J.K., B.C.J., S.G.I., Y.J., J.E.K., and S.-Y.J. Investigation: J.K., D.K., Q.H.N., B.C.J., H.L., J.E., J.E.K., S.-Y.J. Visualization: J.K., D.K., B.C.J., S.G.I., and Y.J. Supervision: B.C.J., S.G.I., and Y.J. Writing—original draft: J.K., B.C.J., S.G.I., and Y.J. Writing—review and editing: J.K., D.K., Q.H.N., C.L., N.K., B.C.J., S.G.I., Y.J., H.L., J.E., J.E.K., and S.-Y.J. **Competing interests:** J.K., D.K., and Y.J. are inventors of a patent application related to this work (10-2024-0032967, Republic of Korea). The other authors declare that they have no competing interests. **Data and materials availability:** All data needed to evaluate the conclusions in the paper are present in the paper and/or the Supplementary Materials.

Submitted 6 March 2024

Accepted 8 July 2024

Published 9 August 2024

10.1126/sciadv.adp0778